GRANT 1 HG
30 pages

FINAL REPORT IN-19600

Analysis of Jovian Decametric Data: Study of Radio Emission Mechanisms

NASA Grant NAGW-373

Covering the period

September 15, 1982 - May 31, 1986

Submitted by

David H. Staelin
Philip W. Rosenkranz
Tomás A. Arias
Peter N. Garnavich
Roel Hammerschlag

(NASA-CR-176878) ANALYSIS OF JOVIAN DECAMTERIC DATA: STUDY OF RADIO EMISSION MECHANISMS Final Report, 15 Sep. 1982 - 31 May 1986 (Massachusetts Inst. of Tech.) 30 p
N86-30619
Unclas
CSCL 03B G3/91 43536

August 12, 1986

Massachusetts Institute of Technology
Research Laboratory of Electronics
Cambridge, Massachusetts 02139

Table of Contents

Analysis of Jovian Decametric Data: Study of Radio Emission Mechanisms

I. Introduction

This research effort involved careful examination of Jovian radio emission data below 40 MHz, with emphasis on the uniquely informative observations of the Planetary Radio Astronomy experiment (PRA) on the Voyager 1 and Voyager 2 spacecraft. The work is divided here into three sections, each addressing a different type of emission. These three sections address decametric "arcs," decametric "V bursts," and hectometric "modulated spectral activity" (MSA), respectively.

II. Jovian Decametric Arcs and Alfvén Currents

One of the unexpected discoveries of the Voyager Planetary Radio Astronomy (PRA) experiment (Warwick et al., 1979a, b) was that the decametric radio emission (DAM) often appeared in the form of "arcs" when displayed in time-frequency coordinates. These arcs are regular in appearance and often occur at intervals of 2 - 20 minutes. A typical PRA record is presented in Figure 1.

Based in part on measurements of electron density in the Io plasma torus by the PRA instrument (Warwick et al., 1979a), Gurnett and Goertz (1981) suggested that the arcs might be produced by separate large electric currents, each associated with the separate reflections from the Jovian ionosphere of the Io-induced Alfvén waves. Multiple reflections could occur because the reflected wave would not be terminated by Io, which would have time to move out of the way before the wave would be reflected by Jupiter. They estimated that the ionospheric impedance was sufficiently low that many tens of reflections could occur as the waves propagate back and forth between hemispheres along those magnetic field lines stimulated by Io's passage.

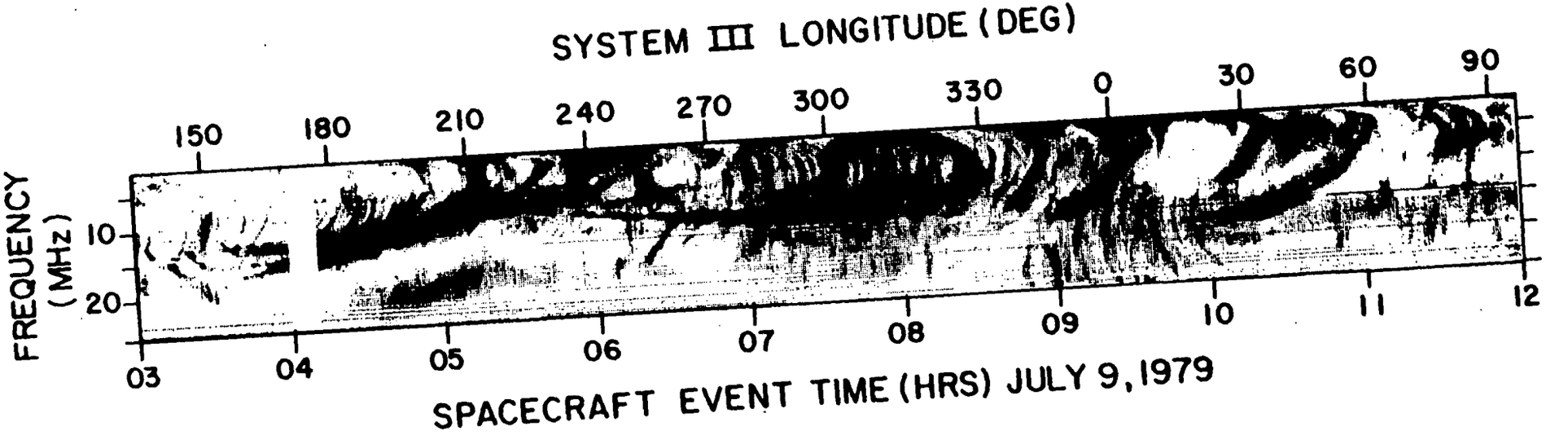

Figure 1. Decametric arcs observed during Jupiter encounter.

Extending this picture, Bagenal (1983) showed that the spacing between currents, and therefore between the arcs, should vary with Jovian longitude as does the average Alfvén velocity, and that the spacing should either increase or decrease systematically as those currents are repeatedly reflected subsequent to Io's passage.

To test all of these conjectures catalogues of Jovian L-burst arcs and of pairs of adjacent arcs were prepared from the Voyager 1 and 2 PRA data. In addition the gaps between adjacent arc-like features in the Jovian decametric S-burst emission were also catalogued (Garnavich, 1983; Leblanc, 1981).

The properties of L-burst arcs were estimated by visual examination of archived PRA "POLLO" spectral data provided by Warwick (personal communication). Such data have been presented elsewhere (Warwick et al., 1979a,b), and are represented here in Figure 1.

Catalogues of 100 representative arcs were prepared for each of Voyager 1 and Voyager 2, and catalogues of 100 gaps between adjacent arcs were similarly prepared for each spacecraft. In each of these four catalogues the events were deliberately distributed approximately evenly over periods of the one to two weeks near encounter. Intervals of an hour or more typically elapsed between the chosen events, although they occasionally were as short as 10 minutes. No rigorous selection protocol seemed practical, and therefore a compromise was made between arc strength and uniformity of distribution in time. Pairs of adjacent arcs were similarly selected to define gaps.

The principal catalogued parameters discussed here are the time, vertex frequency, Jovian longitude, Io phase, and thickness of each arc at the vertex frequency. Vertex frequency is defined to be that midrange frequency at which an arc first or last appears; see Figure 1. Vertex-early and

vertex-late arcs are observed first and last, respectively, at their vertex frequency. The time and coordinates of an arc refer to the middle of the emission observed at the vertex frequency. Jovian longitude is the central meridian longitude of the spacecraft at the time of observation. Estimates of vertex frequency and time occurrences are typically accurate to 1-2 MHz and 1-2 minutes, respectively. Arc gaps were estimated with accuracies of 1 minute or less. Both arcs and arc gaps were categorized by their clarity, and a few of the most questionable entries were omitted from subsequent analyses.

The primary purpose of these catalogues was to illuminate the process of arc formation. The first use of this data was to confirm the earlier observation of Staelin (1981) that most vertex-early and vertex-late arcs were systematically offset in longitude by 120 degrees. The offset is most clearly resolved when the data is displayed as a function of vertex frequency. This earlier result, based on 55 Voyager-1 arcs, has been confirmed and refined by these more careful analyses of the 116 right-circularly polarized Voyager-1 and Voyager-2 arcs, displayed in Figure 2.

The mechanism which relates vertex frequency to longitude is unknown. The offsets between the vertex-early and the vertex-late arcs are 120-140 degrees, consistent with a hollow cone of radio emission aligned with the local magnetospheric field and flared outward at a half angle of $\sim$ 70-90 degrees. The arc shape could plausibly be the result of systematically larger flare angles near the vertex frequency. Possible mechanisms for this have been discussed by Staelin (1981), Goldstein and Thieman (1981), and Pearce (1981), but they remain speculative.

A simple equation for the longitude $Lo(f_v)$ of the presumed cone axis was fitted to the vertex frequency f_v (MHz) for $8 \leq f_v \leq 25$ MHz;

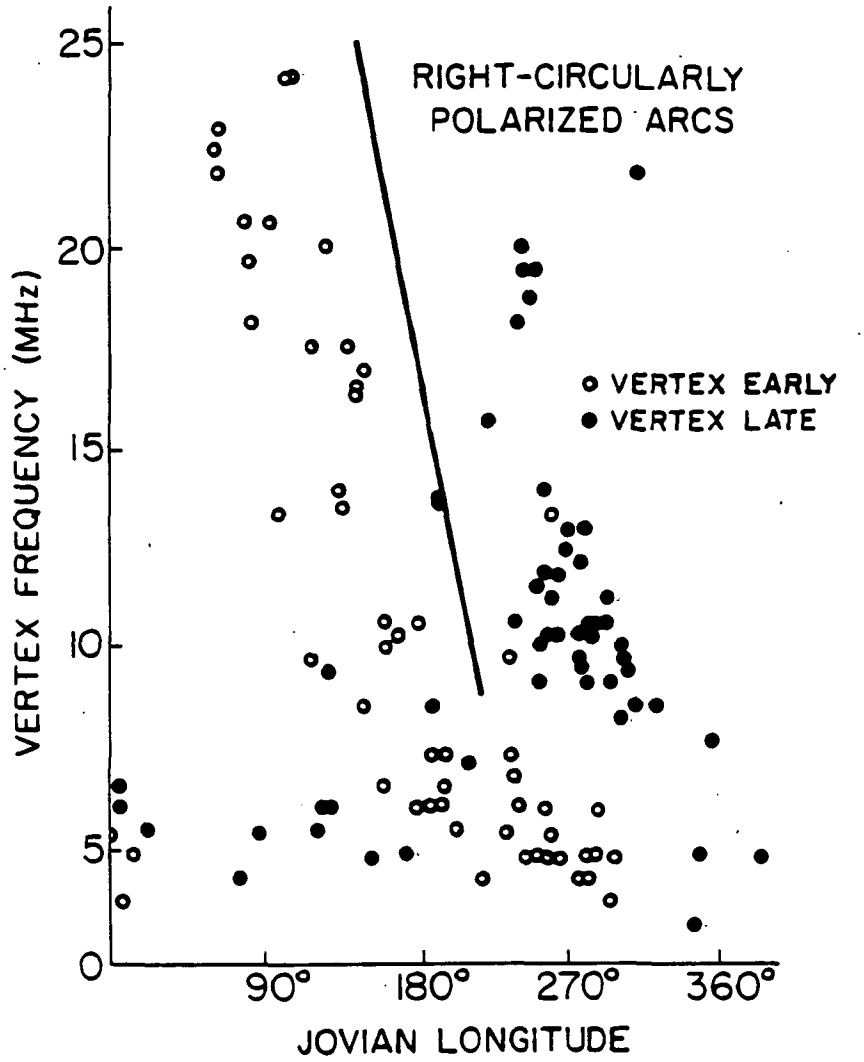

Figure 2. Distribution of vertex frequency for right-circularly polarized arcs as a function of Jovian longitude. The straight line represents the presumed longitude of currents radiating arcs at the indicated vertex frequency.

$$Lo = 256 - 4.56\ f_v \text{ degrees} \qquad (1)$$

The difference between Jovian arc longitude and cone axis longitude $Lo(f_v)$ was then computed for each arc, and the histogram for the arcs appears in Figure 3, where vertex-early and vertex-late arcs are plotted separately. The histogram suggests that typical cone half angles projected on the Jovian equator (i.e. perceived by Voyager) are 50 - 90 degrees, and that they seldom exceed 90 degrees.

The fact that the histograms drop sharply at ± 90 degrees, in contrast to the broad character of the rest of the distribution, suggests that the relation between vertex frequency and longitude may be relatively more stable than the projected cone half angle, which appears to vary ± 20 degrees. It seems plausible that different Alfvén currents might yield quite different cone angles at any given frequency and longitude, as inferred from these data, if cone angles were sensitive to local current densities and energies, plasma frequencies, pitch angle distributions, etc.

In the multiply-reflected Alfvén-wave model for arcs proposed by Gurnett and Goertz (1981), one parameter of interest was the ionospheric reflection coefficient and the resulting lifetime for Io-generated Alfvén waves. Two types of evidence are presented here for long lifetimes; one is the longitudinal distribution with respect to Io of currents that produce arcs, and the other is the average number of arcs visible per degree of longitude; the latter is more ambiguous.

In Figure 4 is plotted the number of arcs observed as a function of the difference in longitude between Io and the Alfvén current that presumably radiated any given arc. Consistent with the arc angle distributions of Figure 3, the longitude of the current was assumed to be +60 degrees or -60 degrees from the arc longitude, depending on whether it

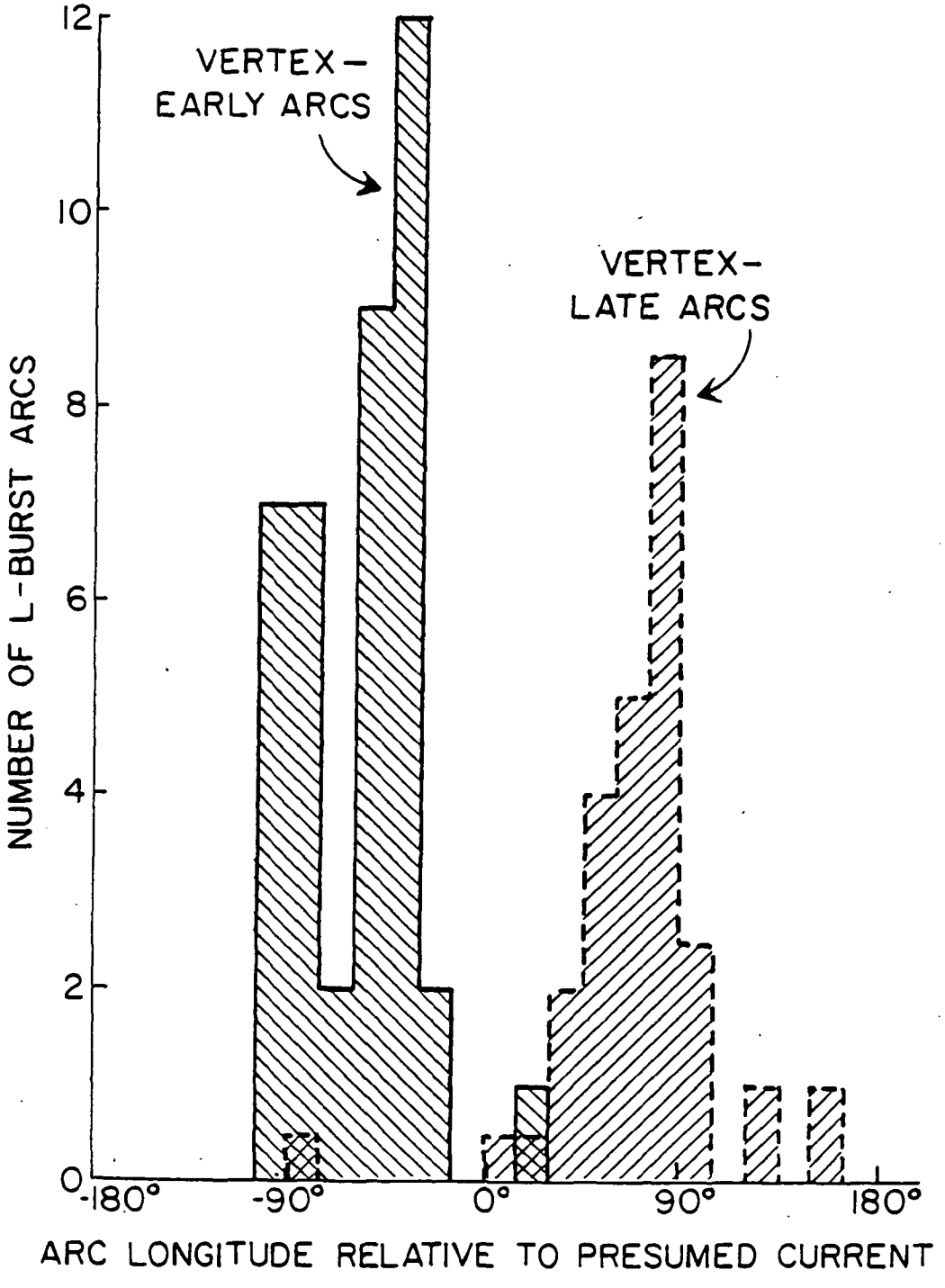

Figure 3. The distribution of observed decametric arc longitudes relative to the longitude of the presumed radiating current.

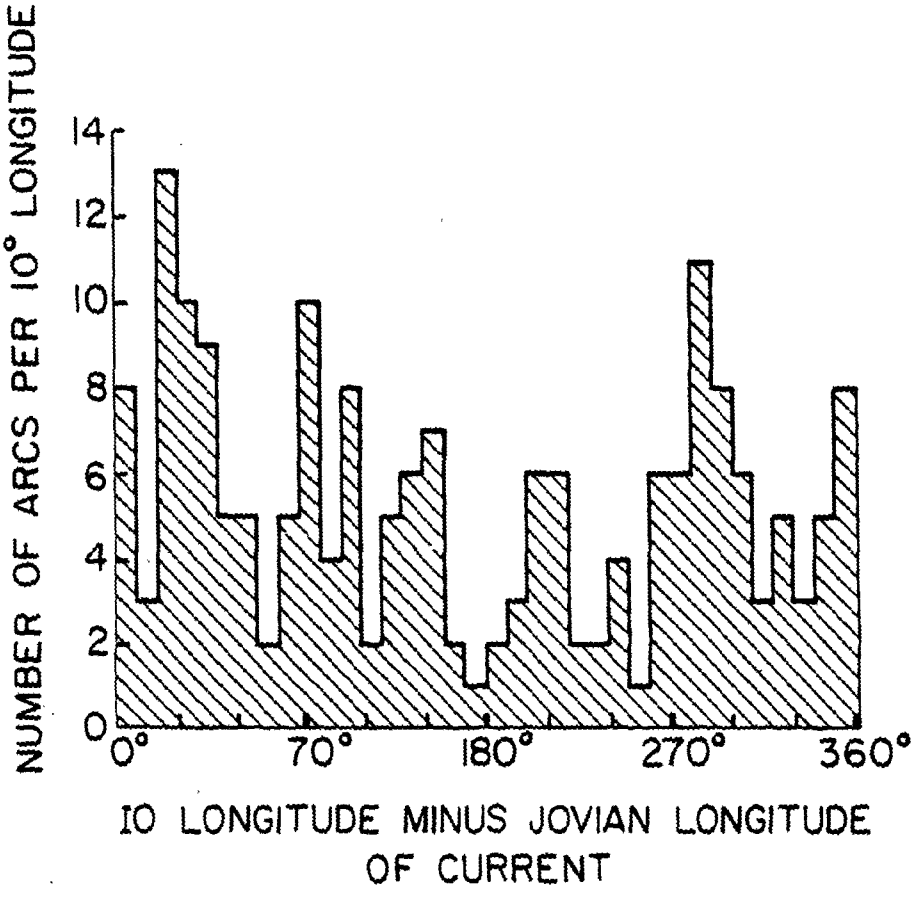

Figure 4. Distribution of observed decametric arcs as a function of the longitude offset between Io and the presumed longitude of the radiating current.

was vertex-late or vertex-early, respectively. In Figure 4 there is no statistically significant tendency for arcs to be produced immediately after Io passage, and thus it seems likely that arcs may be produced even after Io has circulated around Jupiter at least a few times. Although the selection effects in producing the arc catalogue have a small tendency to distribute the observed arcs over all time, the uniformity of the distribution in longitude cannot be explained purely in this way.

Further evidence for the longevity of Alfvén waves can be obtained by examining the average number of arcs observed per degree of longitude. In Figure 5 is presented the theoretically predicted round-trip time for an Alfvén wave moving between Jovian hemispheres along a given field line. The systematic variation with longitude is due primarily to the longitudinal variation of magnetic field strength in the Io plasma torus within that magnetospheric shell traversed by Io. The 04 magnetic field model (Acuna and Ness, 1976) and the Io torus plasma density derived from the Voyager plasma and PRA experiments (Bagenal, 1981) were employed for these calculations.

Because Io simultaneously generates both north- and south-moving Alfvén waves, the basic interval between arcs should average $\sim$ 13 minutes, which is one half the round trip time; the interval depends in part on how well centered Io is within the plasma torus (Bagenal, 1983). Still closer average spacings between arcs can result if the Alfvén waves continue to reflect between hemispheres until Io returns and overlays a second set of waves. The observed density of arcs can thus be one or more times greater than the basic density, depending on how many times Io circulates before the Alfvén currents fade.

In Figure 6 are presented the observed intervals between arc pairs as a function of the presumed Jovian longitude of

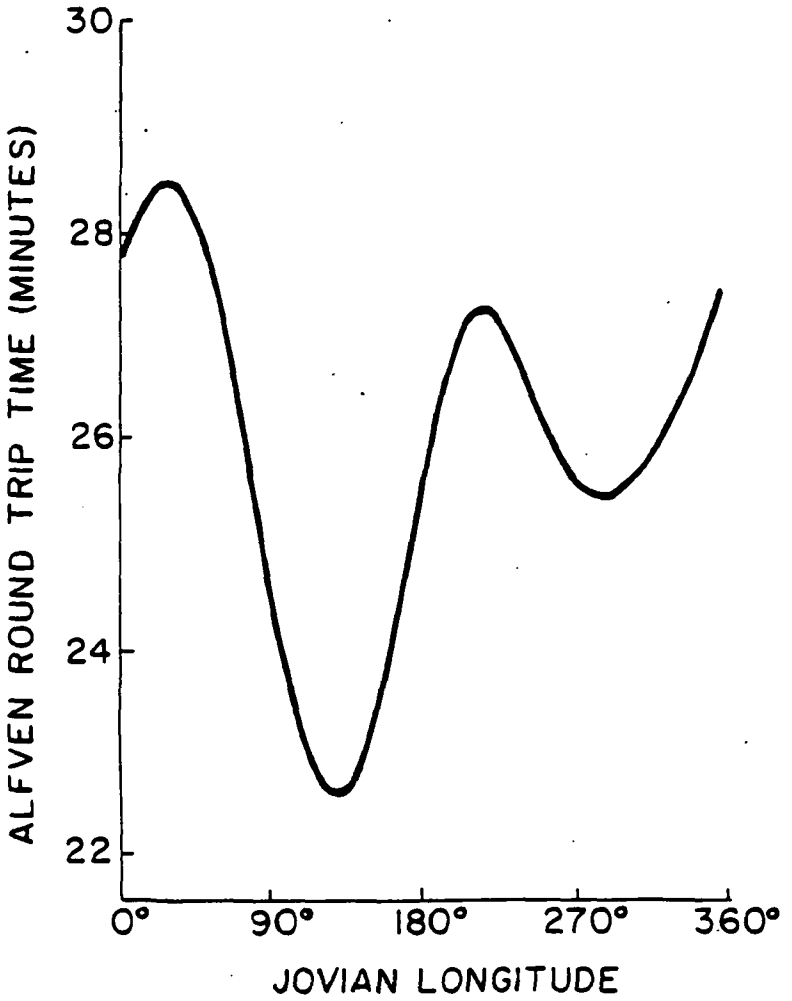

Figure 5. Predicted round-trip time for magnetospheric Alfvén waves excited by Io, as a function of Jovian longitude.

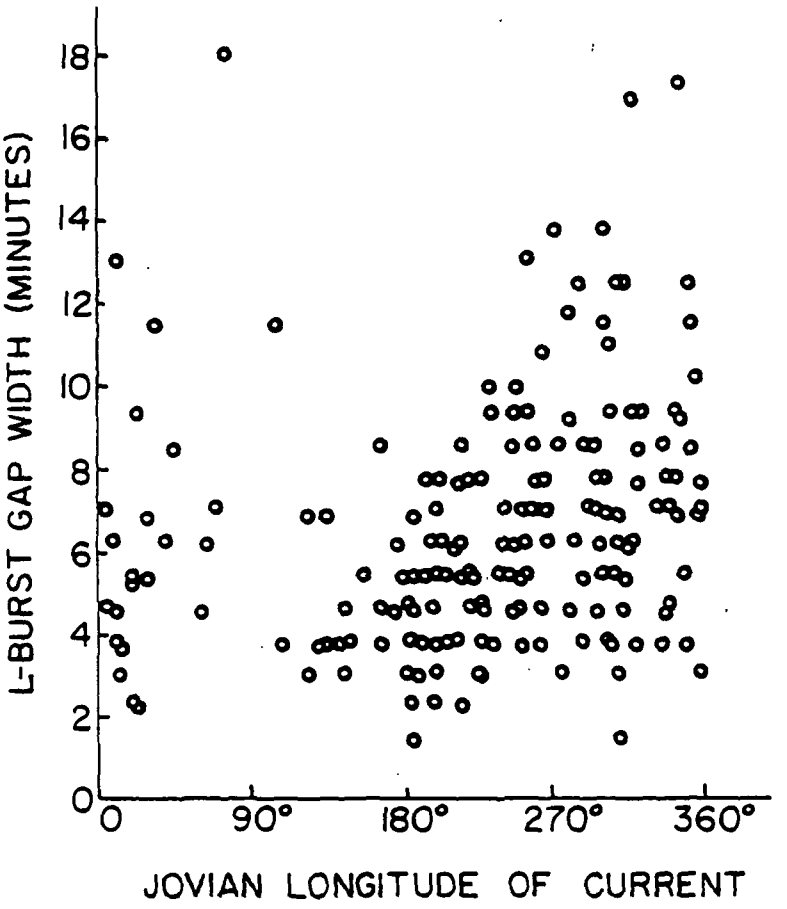

Figure 6. Distribution of the interval between consecutive L-burst arcs, as a function of Jovian longitude.

the radiating current. Typical catalogued arc intervals are only $\sim$ 4-7 minutes, versus $\sim$ 11-14 minutes for the predicted initial intervals, a factor of $\sim$ 2.3 greater. This suggests the effective lifetime of radiating Alfvén currents may be 2-3 Io revolutions, or a few days.

Still longer lifetimes for the Alfvén currents are implied by the statistical distribution of observed arc gap widths. Assume that several overlapped sets of arcs coexist and that arc positions are independent of those associated with previous sets; the resulting arc gaps G should be Poisson distributed, so that the probability $P(G) = \beta \exp(-\beta G)$, where β is the average number of arcs per unit time. In Figure 7 is plotted the natural logarithm of the number of observed arc gaps as a function of gap width. The reduced number of observed gaps narrower than 3 minutes corresponds to the typical width of the arcs; most arcs closer than this could not be resolved. The value of β can be determined directly from the slope of the distribution for gaps longer than 5 minutes, and is approximately 3.2 arcs per minute. This rate is so large that it implies a near continuum of arcs such that observable gaps are more the exception than the rule. Some of the PRA records have this appearance. This extreme density implies that Io may circulate more than 40 times around Jupiter before its Alfvén waves are attenuated, or perhaps a month or more. Alternatively, single Alfvén currents may produce multiple arcs.

This simple picture must be examined more carefully, however. As Bagenal (1983) observed, the fact that the round-trip time R is a function of longitude w implies that the spacing of Alfvén currents can increase or decrease in time, depending on the slope of the function R(w). Such a relation is plotted in Figure 8 for Alfvén currents presumed to flow in the longitude interval 220 - 240 degrees, as a

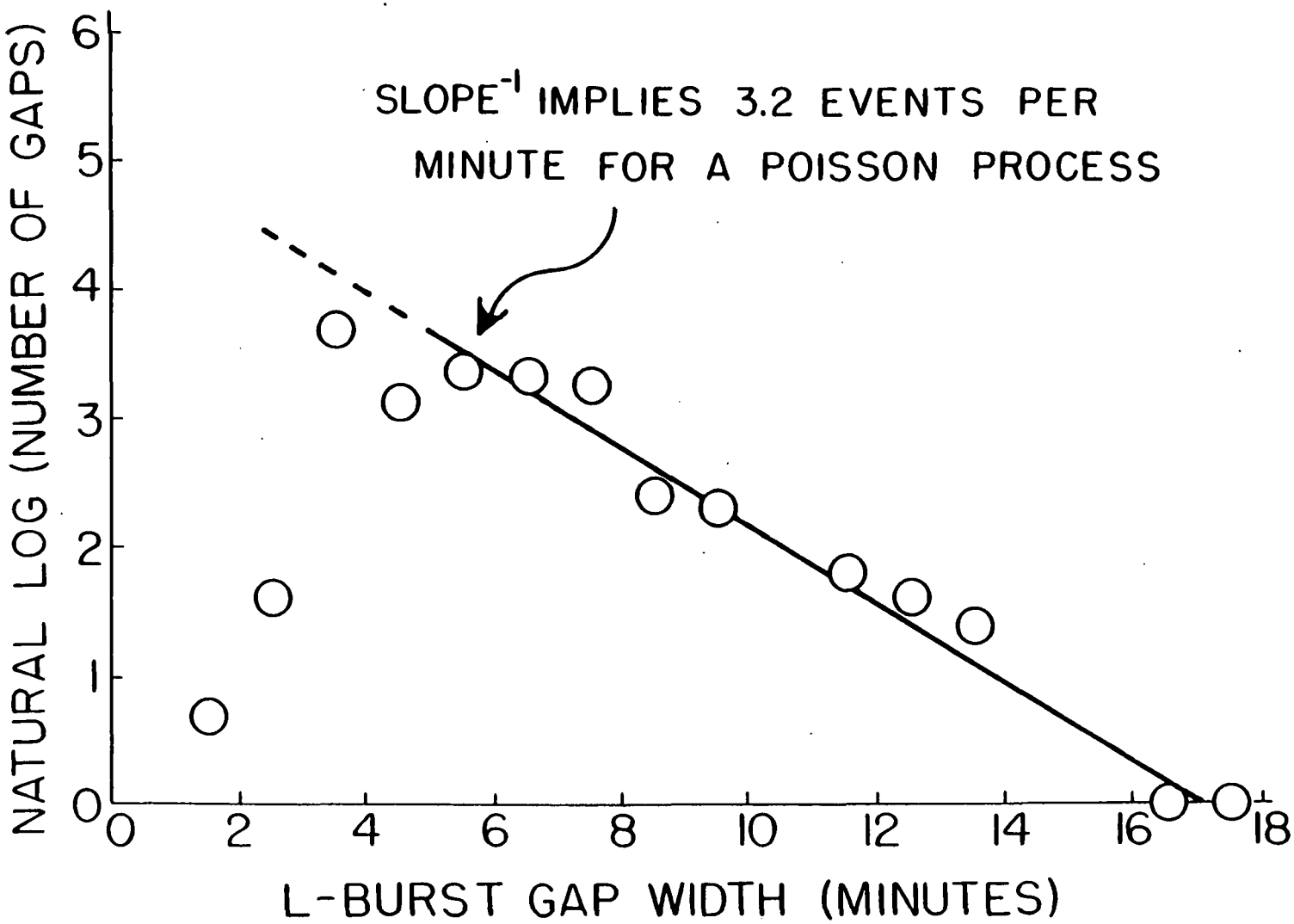

Figure 7. Natural logarithm of the distribution of intervals between consecutive L-burst arcs, as a function of this interval (gap width).

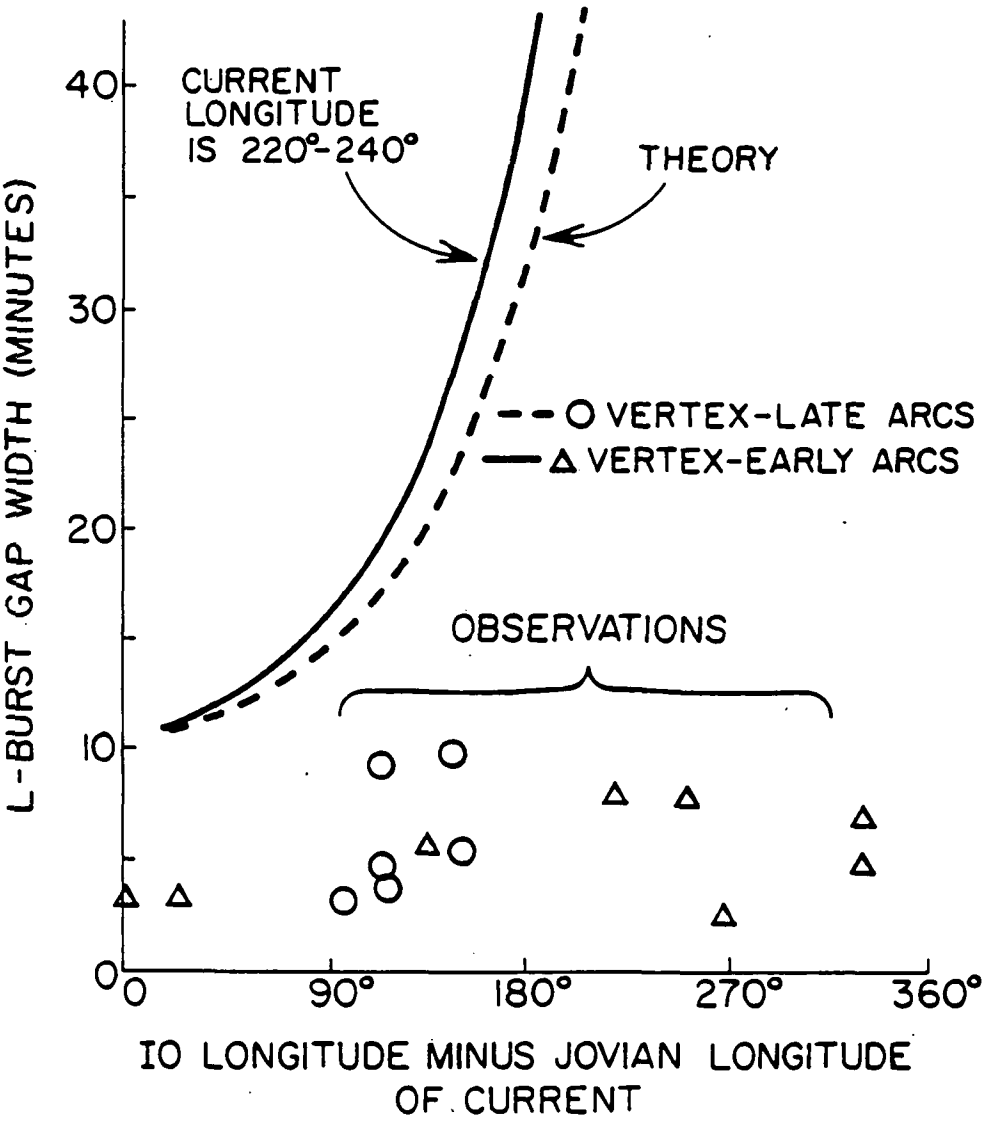

Figure 8. Theoretical and observed L-burst gap widths as a function of offset in longitude between Io and the radiating current.

function of the difference Δ in longitude between Io and the current of interest. In this case the slope is such that the gap width G will approach infinity as Δ increases, and then start to decrease toward zero. At other longitudes the gap G will start to diminish immediately. For longitudes where the derivative of round-trip time with respect to longitude is maximum, this process can result in typical arc gaps of less than a minute within a few revolutions of Io after the Alfvén waves are generated. It is therefore reasonable to conclude that Io circulates at least several times before the Alfvén waves generated at a particular time decay to the point where they no longer radiate observable arcs. This conclusion is also consistent with the results presented earlier in Figure 4.

III. Formation of Jovian Decametric S Bursts by Modulated Electron Streams

Shortly after the discovery of Jovian decametric radiation it was noted that it varied on two different time scales; long "L" bursts varied on scales of seconds or minutes, whereas short "S" bursts varied on a scale of milliseconds (Genova and Leblanc (1981). Individual S bursts furthermore drifted downward in frequency at rates between $\sim$ 5 and $\sim$ 35 MHz s^{-1}, the drift rates in units of MHz s^{-1} typically approximating the emission frequency in units of MHz (Riihimaa, 1977).

This observed strong correlation between drift rate and emission frequency immediately suggested that packets of electrons were moving outward at $\sim$ 0.1 c along the Jovian magnetic field lines and were radiating near their cyclotron frequency. Initially it was proposed that the electron packets were moving adiabatically in trapped orbits, but more recent data near 30 MHz yields the highest drift rates observed, rather than rates approaching zero as one would expect near the mirror point (Leblanc et al., 1980).

Since it appears unlikely that the radiating packets of electrons are moving adiabatically outward from a mirror point, they are very likely accelerated near the ionosphere, perhaps when the Io-induced Alfvén wave is reflected there, as hypothesized by Gurnett and Goertz (1981).

We assume here that electrons accelerated near the ionosphere move outward along the magnetic field lines nearly adiabatically and with only modest conversion of longitudinal energy to transverse energy due to various plasma interactions. A modest fraction of that transverse energy is then converted to electromagnetic radiation. We further assume that this acceleration is concentrated in a zone near the ionosphere and consists of a steady term plus components at $\sim$ 1-100 Hz. These simple assumptions lead to predictions of complex behavior for S bursts, much of which has already been observed. They further lead to more precise statements about the spatial distribution of radiating electrons.

Consider a linear electron beam at time t passing some point s = 0 with velocity v(t) in the +s direction where v(t) fluctuates about some average value v_o. We may view the spatial distributions of electrons at subsequent times in the reference frame moving with the beam at velocity v_o, as illustrated in Figure 9.

The principal feature of such velocity modulation is that such a beam of ballistic electrons eventually forms cusps of extreme electron density that move and may disappear with time. Cusps occur where the beam distribution function $\Delta s(t)$, illustrated in Figure 9, folds back on itself. It is these cusps that we associate with S bursts.

Early observations of S bursts revealed that they drifted at diverse rates generally correlated with the radio frequency. Groth and Dowden (1975) first noted that S bursts observed at

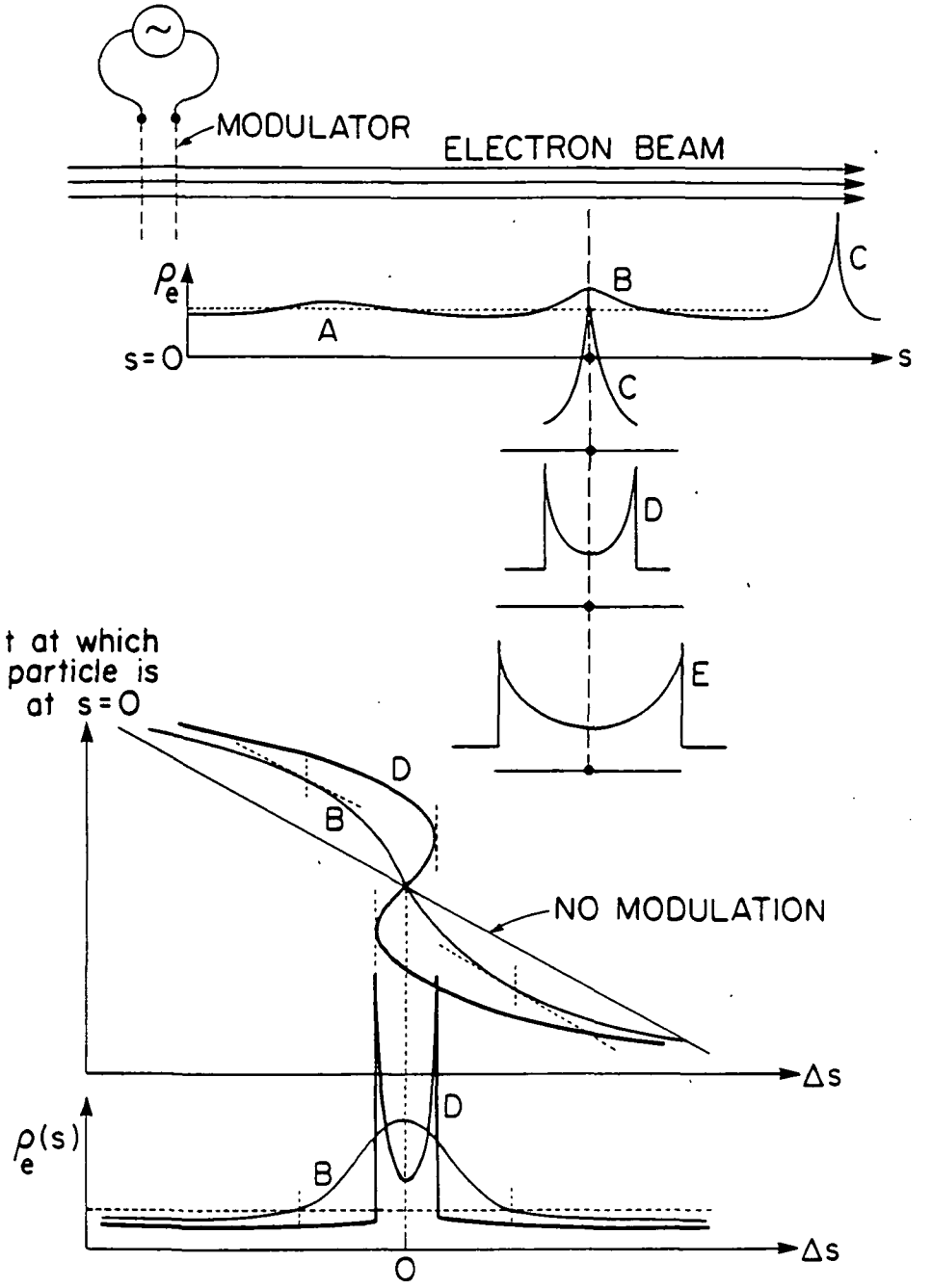

Figure 9. Formation of electron density cusps in a velocity-modulated electron beam moving in the +s direction. At time t the electron density $\rho_e(s)$ for five packets (A-E) is illustrated. The density first becomes singular for packet C, where the cusp first forms; cusp C will bifurcate as it moves in the +s direction, evolving into the forms D,E. The distance measured in the frame of reference moving with the average beam velocity is represented by Δs; with no modulation, Δs of an electron varies linearly with the time t at which it passed s = 0. With modulation this relationship $\Delta s(t)$ is graphed for cusps B and D together with the corresponding $\rho_e(\Delta s)$.

23-25 MHz often occurred in diverging pairs that could be inferred to intersect at frequencies near 32 MHz. Leblanc et al. (1980) and Riihimaa and Carr (1981) also have observed V bursts. Two-to-one drift rate ratios were observed by Leblanc et al. (1980) in the band 15-35 MHz, and comparable values, sometimes less, are evident in the figures of Riihimaa and Carr (1981). These ratios correspond to peak modulating voltages of $\sim$ 1.5 kV, or $E \gtrsim 10^{-3}$ V m^{-1}.

This hypothesis for emission of S bursts by transient electron density cusps makes a specific prediction that can be partially tested; the radiation intensity in the time-frequency plane should appear V shaped with some intensity inside the "V" near the vertex, but much less outside the V. This follows because the radiation intensity is presumably related monotonically to the local hot electron density, and therefore the intensity patterns of V bursts should resemble the electron density distributions suggested in Figure 9. The filled-V form is strongly suggested in S-burst data presented in Figure 1b of Leblanc et al. (1980), but additional measurements to quantify this would be helpful.

The coherence of the electrons in the emitting cusps can be estimated by assuming that the beam density there is $\sim$ 15 cm^{-3} and that the entire $\sim 5 \times 10^6$ A current participates in radiating the observed $\sim 3 \times 10^8$ W of S-burst emission. If the electrons have a transverse energy of $\sim$ 200 eV, then one perfectly coherent cube of n_c such electrons (15 cm^{-3}) $\lambda/3$ on a side could radiate $\sim 2 \times 10^{-5}$ W at a typical frequency of 16 MHz. If one half of the beam electrons are in such cusps, and if radiation from the coherent cubes combines incoherently, then total S burst power would be $\sim 8 \times 10^9$ W. Note that this total power is not a strong function of the coherence between cubes because the cubes are comparable to a wavelength in size. In this simple example $\sim$ 4% of the cusp electrons need to be

coherent to produce the observed $\sim 3 \times 10^8$ W of S burst power. This large percentage again supports the notion that a large fraction of the $\sim 5 \times 10^6$ A current must be modulated and produce S bursts, and that the cusp electron density must approach the density of the background magnetospheric plasma.

When a cusp forms, becomes coherent, and then bifurcates, the electrons located between the cusps generally are not observed in emission except near the vertex of the V, as noted earlier. The V-burst shadow events observed by Riihimaa and Carr (1981) and by Riihimaa et al. (1981) suggest, however, that these electrons between cusps retain their coherence at least for some time after their direct emission becomes unobservable. Shadow bursts are produced when V bursts occur simultaneously with L bursts; the V burst suppresses the L burst and produces a V-shaped "shadow." The shadows are dark across the entire V, forming a dark triangle. Sometimes the edges of the V burst are sufficiently bright to be seen, but the central region is always suppressed. The suppression of shadow events across the entire V is further evidence that there are excess electrons between the walls of the V, as predicted by this ballistic hypothesis and suggested by Riihimaa et al. (1981) on the basis of their data.

The V bursts might suppress the L bursts when the V-burst electron density cusps move through the emission region and, due to Doppler and other effects, disrupt the coherence of the L-burst electrons, as suggested by Riihimaa and Carr (1981); this L-burst coherence is evidently reestablished within a couple of milliseconds, and the L burst continues exactly as before. The fact that L bursts are strong in frequency bands that persist for seconds or minutes suggests that the coherence mechanism may arise from instabilities in distributions of electrons that are near their mirror point and are also concentrated to high densities, although this L-burst coherence mechanism can evidently be overwhelmed by the local fields of passing S-burst electron packets.

Shadow bursts thus suggest that S bursts and L bursts can arise from two unstable populations of electrons coexisting briefly in one place and that the S-burst packets carry their own coherence mechanism. If the S-burst packets do provide their own coherence, as seems likely, then their Doppler-shifted cyclotron frequency will be above all resonances of the ambient plasma within some cone angle of emission (Staelin, 1981), and possible angles are comparable to those observed. The S-burst emission cones deduced from observations (Leblanc and Genova, 1981) are very similar, although not identical, to those deduced for L bursts.

This study of V bursts has been documented further by Staelin and Rosenkranz (1982).

IV. Hectometric Jovian Modulated Spectral Activity

Although it has long been known that Jupiter emits strongly at hectometric wavelengths, one interesting form of emission remained obscure until the initial spectral data in POLLO mode were displayed with a resolution of 6 seconds, rather than of 48 seconds. The resulting spectra exhibit strong quasiperiodic modulation in frequency with periods lying between $\sim$ 50 and $\sim$ 300 kHz; 150 kHz is typical. This emission, designated "Modulated Spectral Activity" (MSA), drifts slowly and randomly in frequency such that the modulation is often obscured at 48-second resolution.

Typical MSA storms last several minutes or more, and occur between $\sim$ 200 and $\sim$ 1.3 MHz; although these storms sometimes appear to extend above 1.3 MHz, the PRA instrument has insufficient spectral resolution above 1.3 MHz to resolve the modulation lines. The PRA polarization data reveal only scrambled behavior, no systematic polarization structure has yet been identified.

Because the phenomenon must be displayed properly to be most evident, these techniques are summarized below together with the instrument characteristics.

The PRA instrument consists of a pair of orthogonal 10-m monopole antennas and a 198-channel superheterodyne receiver which together measure both modes of circular polarization. The PRA channels are organized into a low-frequency (LF) band, (1.2 kHz-1.3 MHz), and a high-frequency (HF) band, (1.2 MHz-40.5 MHz). The HF band contains 128 200-kHz-bandwidth channels spaced at 307.2 kHz intervals. The 70 LF 1-kHz-bandwidth channels are positioned between the spacecraft power supply harmonics at 19.2 kHz intervals. Thus, due to reduced spacecraft interference, the LF band offers greater frequency resolution and higher sensitivity than the HF band. The system has several modes of operation; for more detailed descriptions see Warwick et al. (1977) and Lang and Peltzer (1977).

In the polarization low-bit rate (POLLO) mode the receiver scans through 198 discrete frequencies once every 6 seconds, alternating the polarization mode measured with each step in frequency and alternating with each scan the mode observed for a fixed frequency. The receiver dwells at each frequency for 25 ms after a 5-ms settling time; the remaining 60 ms per scan are used for bookkeeping operations. The data thus gathered are then transmitted back to earth where they are recorded in a logarithmic scale on magnetic tape.

Plots of the sum of left-hand (LH) and right-hand (RH) circular flux density are made with 6-s resolution (24 min duration). Only one polarization mode is recorded in each channel and the recorded mode alternates from channel to channel (LH RH LH RH etc.). The density of the unrecorded polarization mode in each channel is estimated by averaging the values recorded in the immediate neighbors of the channel in question. Then, to insure that every channel's full dynamic range is visible in the plots, each channel is assigned a separate logarithmic gray-scale (linear in the values recorded

on tape), where white represents the channel's lowest value during the 24-minute period, and the channel's mean is represented by a gray-level fixed for all channels and chosen so that 2.5% of all values presented in each plot are lost to saturation (black). This last criterion avoids setting the gain artificially low to accommodate strong or infrequent noise bursts. Each channel's mean is computed as the average logarithm of the flux densities computed for that channel during the 24-minute plot; in this average those flux densities substantially above an approximation of the mean are given reduced weight by multiplying them with a Gaussian taper.

Figure 10 illustrates some of the forms in which MSA can occur. Note that the nominal period (in frequency) and drift rate can vary from storm to storm, or even within a single storm. Also note that there is little evidence for multiple storms being superimposed. The stable bands of MSA near zero drift rate are inconsistent with the hypothesis that MSA is merely aliased time modulation; zero average drift rates are too improbable if time modulation of broadband emission is responsible.

Figure 11 presents a summary of MSA detections as a function of spacecraft and Io central meridian longitude (CML). Note that there is no evident dependence on Io and only a weak dependence on spacecraft CML -- there is somewhat less emission for $200 \lesssim$ CML $\lesssim 360°$

Figure 12 illustrates another characteristic of MSA; it sometimes resembles an asymmetric sawtooth wave with its sharp side at lower frequencies. Physical explanations for this asymmetry are difficult to find. Magnetospheric plasma waves generally propagate too rapidly to be consistent with this stable emission characteristic, and magnetospheric electrons near a mirror point would more likely exhibit a sharp void for altitudes below (and frequencies above) the mirror point. The

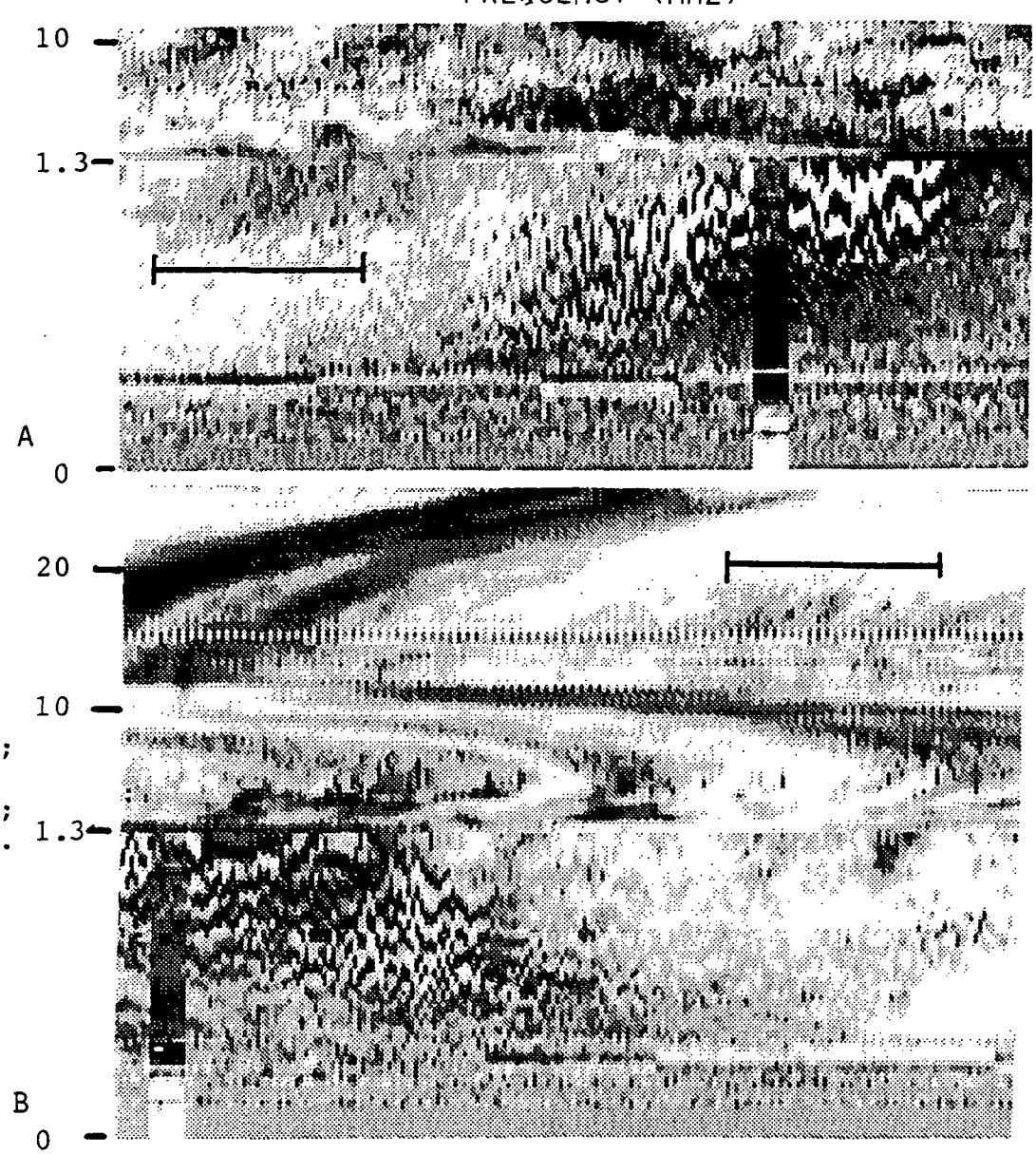

Figure 10. Examples of Jovian MSA. The time bars represent 5 minutes; time increases to the left. Black is more intense emission. Each 6-sec POLLO spectrum is shown. A) Day 57, 13.7 hr; B) Day 59, 19 hr; C) Day 59, 19.4 hr; D) Day 57, 14.8 hr.

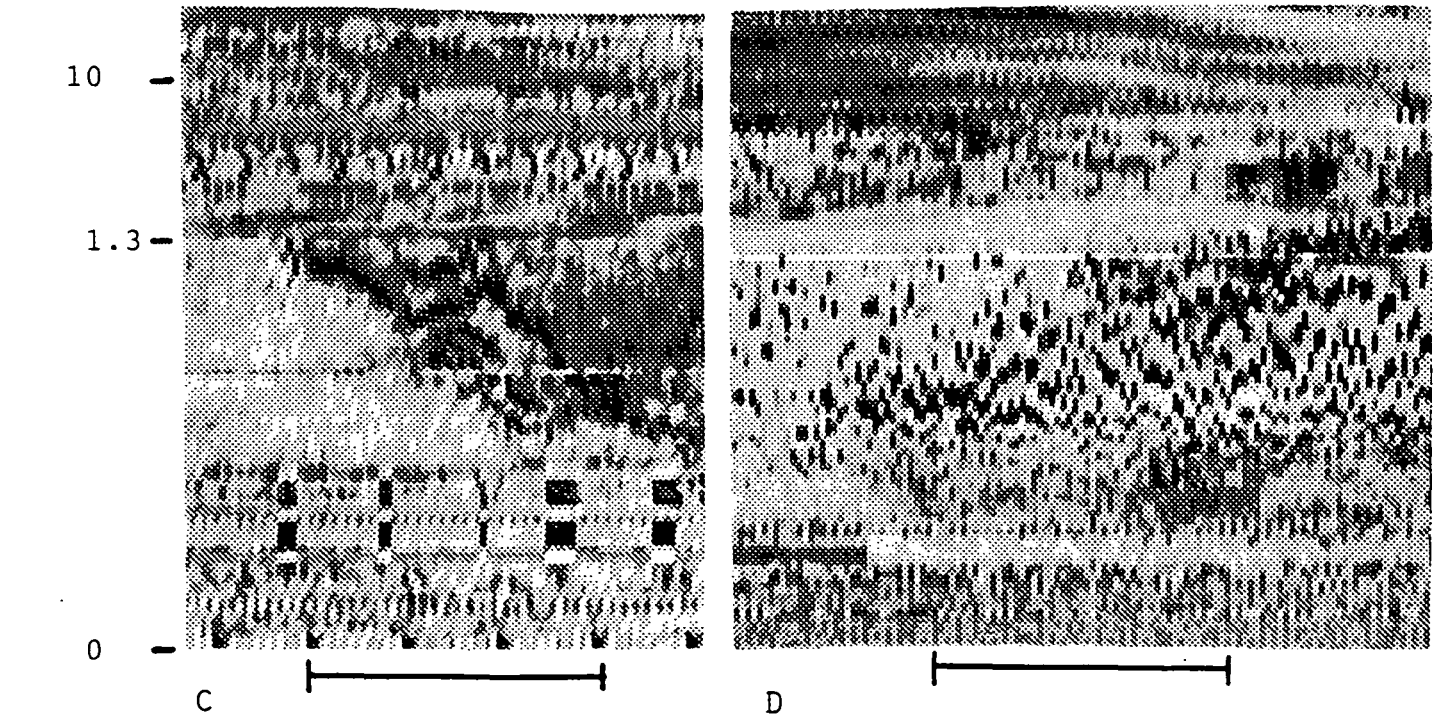

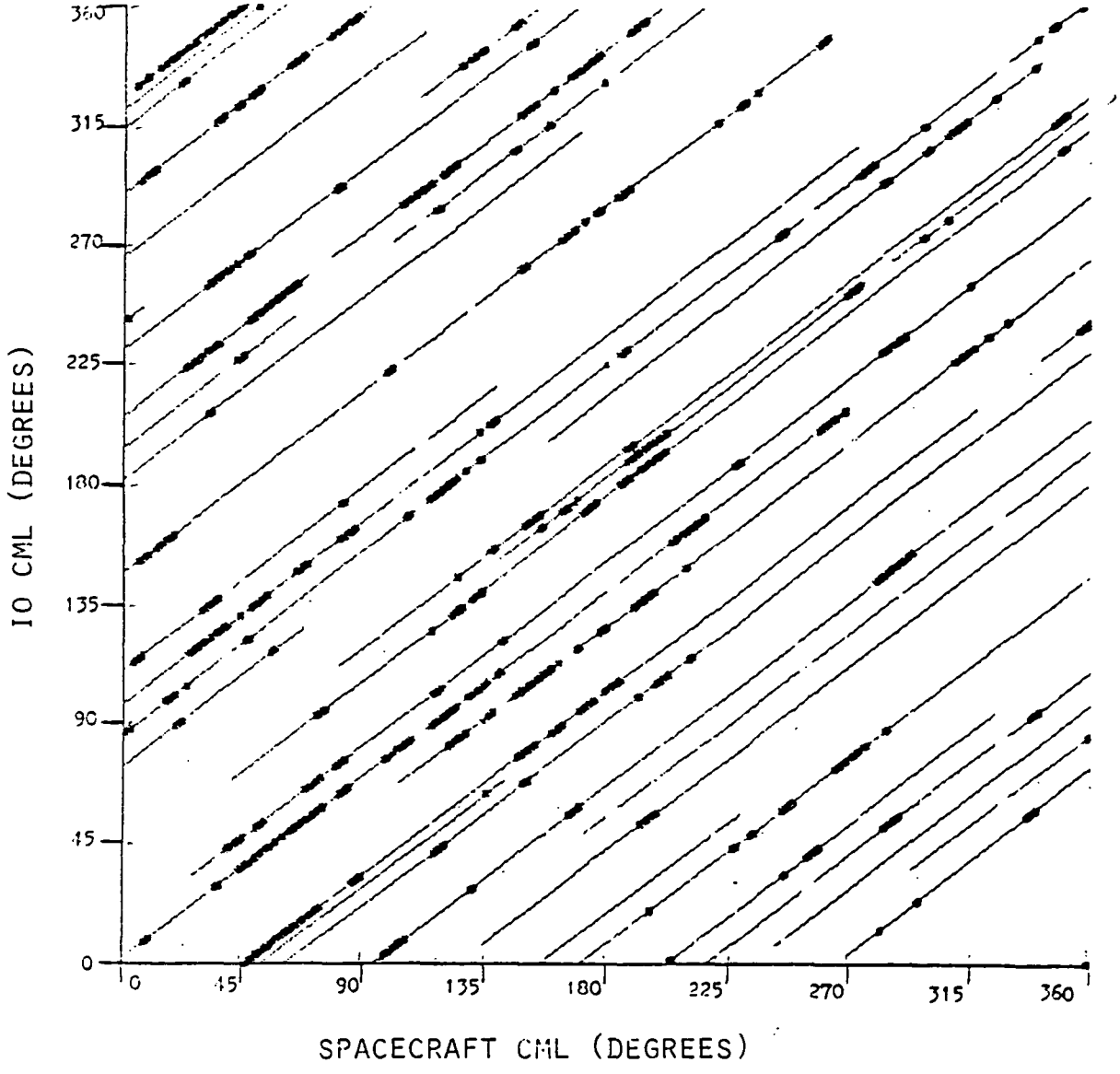

Figure 11. Observations of MSA as a function of spacecraft and Io CML. Regions covered by survey appear as lines which thicken where MSA is observed.

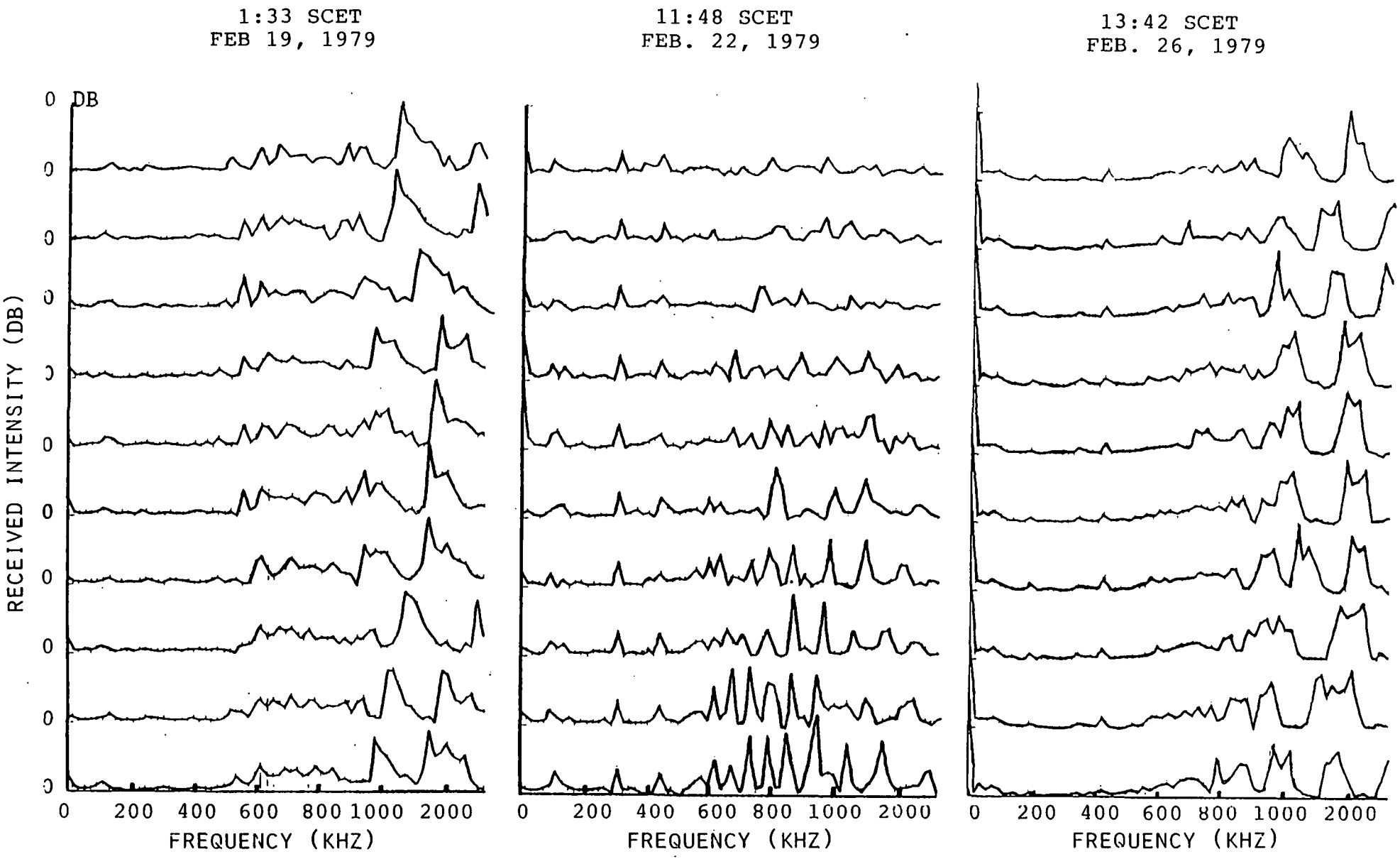

Figure 12. Representative MSA normalized intensity records for consecutive 6-sec intervals; the peak amplitudes are typically 30 dB above the minima. Note the variations in MSA period, spectral shape, and spectral drift; some small stable features represent instrumental effects or interference.

periodic character of MSA would furthermore require a periodic series of mirror points in order for this model to work.

Thus no simple explanation for MSA presently exists. It is not even clear whether it results from a single point source that radiates nearly isotropically, or from many Jovian longitudes with highly beamed emission. It does seem likely that it is emitted from the magnetosphere near the local electron cyclotron frequency, however, largely because of plausibility and because during encounter MSA disappeared while Voyager was concealed (at these frequencies) behind and inside the plasma torus, which refracts strongly radiation in the 200-1000 kHz region.

Much of this work was reported by T. A. Arias ("Modulated Spectral Activity in the Inner Jovian Magnetosphere," S.B. thesis, MIT, Department of Physics, June, 1986).

References

[1] Acuna, M. H., and N. F. Ness, The main magnetic field of Jupiter, J. Geophys. Res., 81, 2917, 1976.

[2] Bagenal, F., The inner magnetosphere of Jupiter and the Io plasma torus, Ph.D. thesis, MIT, Dept. of Physics, 1981.

[3] Bagenal, F., Alfvén wave propagation in the Io plasma torus, J. Geophys. Res., 88, 3013, 1983.

[4] Garnavich, P. M., Jovian decametric radiation: a test of the multiple reflection Alfvén wave model, S.M. thesis, MIT, Dept. of Physics, June 1983.

[5] Genova, F., and Y. Leblanc, Interplanetary scintillation and Jovian DAM emission, Astron. Astrophys., 98, 133-139, 1981.

[6] Goldstein, M. L., and J. R. Thieman, The formation of arcs in the dynamic spectra of Jovian decametric bursts, J. Geophys. Res., 86, 8569, 1981.

[7] Groth, M. J., and R. L. Dowden, Spectra of high-frequency radio emission from Jupiter, Nature, 255, 382-384, 1975.

[8] Gurnett, D. A., and C. K. Goertz, Multiple Alfvén wave reflections excited by Io: Origin of the Jovian decametric arcs, J. Geophys. Res., 86, 717-722, 1981.

[9] Leblanc, Y. (personal communication).

[10] Leblanc, Y., M. G. Aubier, C. Rosolen, F. Genova, and J. de la Noë, The Jovian S-bursts, II, Frequency drift measurements at different frequencies throughout several storms, Astron. Astrophys., 86, 349-354, 1980.

[11] Leblanc, Y., and F. Genova, The Jovian S-burst sources, J. Geophys. Res., 86, 8564-8568, 1981.

[12] Pearce, J. B., A heuristic model for Jovian decametric arcs, J. Geophys. Res., 86, 8579, 1981.

[13] Riihimaa, J. J., S-bursts in Jupiter's decametric radio spectra, Astrophys. Space Sci., 51, 363-383, 1977.

[14] Riihimaa, J. J., and T. D. Carr, Interaction of S- and L-bursts in Jupiter's decametric radio spectra, Moon Planets, 25, 373-387, 1981.

[15] Riihimaa, J. J., T. D. Carr, R. S. Flagg, W. B. Greenman, P. P. Gombola, G. R. Lebo, and J. A. Levy, Fast-drift shadow events in Jupiter's decametric radio spectra, Icarus, 48, 298-307, 1981.

[16] Staelin, D. H., Character of the Jovian decametric arcs, J. Geophys. Res., 86, 8581-8584, 1981.

[17] Staelin, D. H., and P. W. Rosenkranz, Formation of Jovian decametric S bursts by modulated electron streams, J. Geophys. Res., 87, 10,401-10,406, 1982.

[18] Warwick, J. W., J. B. Pearce, A. C. Riddle, J. K. Alexander, M. D. Desch, M. L. Kaiser, J. R. Thieman, T. D. Carr, S. Gulkis, A. Boischot, C. C. Harvey, and B. M. Pedersen, Voyager 1 planetary radio astronomy observations near Jupiter, Science, 204, 995-998, June 1979.

[19] Warwick, J. W., J. B. Pearce, A. C. Riddle, J. K. Alexander, M. D. Desch, M. L. Kaiser, J. R. Thieman, T. D. Carr, S. Gulkis, A. Boischot, Y. Leblanc, B. M. Pedersen, and D. H. Staelin, Planetary radio astronomy observations from Voyager 2 near Jupiter, Science, 206, 991-995, November 1979.